



1 **Spatial Extent of New Particle Events over the Mediterranean**
2 **basin from multiple ground-based and airborne**
3 **measurements**

4 Kevin Berland¹, Clémence Rose¹, Jorge Pey², Anais Culot¹, Evelyn Freney¹, Nikolaos
5 Kalivitis³, Giorgios Kouvarakis³, José Carlos Cerro⁴, Marc Mallet⁵, Karine Sartelet⁶, Matthias
6 Beckmann⁷, Thierry Bourriane⁸, Greg Roberts⁸, Nicolas Marchand², Nikolaos Mihalopoulos^{3,9}
7 and Karine Sellegri¹

8 ¹Laboratoire de Météorologie Physique, CNRS UMR 6016, Université Blaise Pascal, Aubière, France

9 ²Aix-Marseille Université, CNRS, LCE, UMR 7376, 13331, Marseille, France

10 ³Environmental Chemical Processes Laboratory, University of Crete, Heraklion, Crete, 71003, Greece

11 ⁴Laboratory of Environmental Analytical Chemistry, Illes Balears University, Palma, 07122, Spain

12 ⁵Laboratoire d'Aérodologie (LA), Université de Toulouse, CNRS, Toulouse, France

13 ⁶CEREA, joint laboratory Ecole des Ponts ParisTech - EDF R&D, Université Paris-Est, 77455
14 Champs sur Marne, France.

15 ⁷Laboratoire Interuniversitaire des Systèmes Atmosphériques (LISA), UMR-CNRS 7583, Université Paris-Est-
16 Créteil (UPEC) et Université Paris Diderot (UPD), Institut Pierre Simon Laplace (IPSL), Créteil, France

17 ⁸Centre National de Recherches Météorologiques, Météo-France, Toulouse, URA1357, France

18 ⁹IERSD, National Observatory of Athens, P. Penteli, 15236, Athens, Greece

19 *Correspondence to:* Karine Sellegri (K.Sellegri@opgc.cnrs.fr)

20 **Abstract.** Over the last two decades, new particle formation (NPF), i.e. the formation of new particle clusters
21 from gas-phase compounds followed by their growth to the 10-50 nm size range, has been extensively observed
22 in the atmosphere at a given location, but their spatial extent rarely assessed. In this work, we use aerosol size
23 distribution measurements performed simultaneously at Ersa (Corsica) and Finokalia (Crete) over a one-year
24 period for analyzing the occurrence of NPF events in the Mediterranean area. The geographical location of these
25 two sites, as well as the extended sampling period allow us to assess the spatial and temporal variability of
26 atmospheric nucleation at a regional scale. Globally, Finokalia and Ersa show similar seasonalities in the
27 monthly average nucleation frequencies, growth rates, and nucleation rates although the two stations are located
28 more than 1000 km away from each other. Within this extended period, aerosol size distribution measurements
29 were performed during an intensive campaign (July 3rd to August 12th 2013) from a ground based station on the
30 island of Mallorca, as well as onboard the ATR-42 research aircraft. This unique combination of stationary and
31 mobile measurements provides us with detailed insights into the horizontal and vertical development of the NPF
32 process on the daily scale. During the intensive campaign, nucleation events occurred simultaneously both at
33 Ersa and Mallorca over delimited time slots of several days, but different features were observed at Finokalia.
34 The results highlight that the spatial extent of the NPF events over the Mediterranean Sea might be as large as
35 several hundreds of kilometers, mainly determined by synoptic conditions. Airborne measurements gave
36 additional information regarding the origin of the clusters detected above the sea. The selected cases depicted



37 contrasting situations, with clusters formed in the marine boundary layer or initially nucleated above the
38 continent or in the Free Troposphere (FT) and further transported above the sea.

39

40 **1 Introduction**

41 New particle formation (NPF) events have been widely observed in the atmosphere in different environments
42 (Kulmala et al., 2004) from remote areas at high altitude or latitude to polluted environments in different
43 climates (Cusack et al., 2013; Manninen et al., 2010; Pey et al., 2008; Yli-Juuti et al., 2011). However, the exact
44 mechanism and chemical species involved in the NPF process are not fully identified, especially regarding the
45 diversity of environments to consider. Thus most global climate models still do not represent well this process,
46 using parameterizations which are based upon a limited number of mechanisms and gaseous precursors, even
47 though they predict that it may contribute to a significant fraction of condensation nuclei (CN) and cloud
48 condensation nuclei (CCN) concentration at the global scale (Makkonen et al., 2012; Merikanto et al., 2009;
49 Spracklen et al., 2008).

50 The different features of NPF events (frequency, intensity, duration etc...) may be influenced by meteorological
51 variables (temperature, relative humidity and solar radiation) (Birmili et al., 2003; Jeong et al., 2004; Sihto et al.,
52 2006; Young et al., 2007), but also by the availability of gaseous precursors, regarding both their nature and their
53 amount. It is thus necessary to describe the occurrence and characteristics of NPF over a large variety of
54 environments, and assess to what spatial extent these features can be applied to. Although the characteristics of
55 the NPF events have often been documented in the literature (Hirsikko et al., 2007; Manninen et al., 2010; Yli-
56 Juuti et al., 2009, 2011), analysis dedicated to their spatial extent are rare. This might be explained by the fact
57 that such studies require airborne measurements (Crumeyrole et al., 2010; Rose et al., 2015) or multi-sites
58 datasets. Such datasets were analyzed by Hussein et al. (2009) who reported that NPF could take place in the
59 form of regional events over up to thousand kilometers in Scandinavia. Likewise, Dall'Osto et al. (2013)
60 observed regional NPF events occurring in the North-East of Spain. Using a similar methodology, Crippa and
61 Pryor, (2013) observed horizontal extents of a hundred kilometers for the NPF process in USA and Canada.
62 They also pointed out a significant variability of the NPF characteristics (formation and growth rates) within
63 these large scale events, suggesting that local signatures could superimpose to favorable synoptic conditions. In
64 order to allow for the analysis of the horizontal extent of NPF on a single station dataset, different methods based
65 on air mass back trajectory analysis and particle growth rates were also recently proposed (Kristensson et al.,
66 2014; Rose et al., 2015). The Nanomap tool developed by Kristensson et al., (2014) was reported to allow the
67 identification of nucleation areas up to 500 km far from the observation site. The main limitation of this last
68 method is due to the fact that the determination of the nucleation area directly depends on event characteristics
69 that sometimes cannot be accurately defined (i.e. the determination of the end of the nucleation process itself, or
70 the end of the growth process).

71 These few studies dedicated to the analysis of the horizontal extent of NPF were mainly conducted above
72 continental regions. Similar analysis in marine environments are crucially missing although they are of high
73 interest, as it was previously shown that in such pristine environments, cloud properties could be significantly
74 impacted by changes in the aerosol loading (Koren et al., 2014; Rosenfeld et al., 2014; Tao et al., 2012).
75 Although the Mediterranean area is particularly sensitive to the future evolution of atmospheric pollutants and



76 climate change, only a few studies relative to NPF in this area have been reported so far. Intensive campaigns
77 were conducted on the eastern Spanish coast, in Barcelona and at Montseny site (Cusack et al., 2013; Pey et al.,
78 2008), while long-term measurements are performed at the Finokalia (Crete) station (Kalivitis et al., 2008, 2012,
79 2015; Manninen et al., 2010; Pikridas et al., 2012). Frequencies of NPF were reported to range between 25% and
80 36%. The Mediterranean basin is at the cross section of many different influences: there is a strong
81 anthropogenic influence from densely populated coastal zones, which superimpose with marine and dust sources,
82 as well as with emissions from Mediterranean forests and shrublands that emit both terpenes and isoprene. This
83 geographical area is particularly exposed to high radiation compared to the rest of Europe, so that we expect a
84 strong contribution from photochemical processes.

85 In the framework of the projects CHARMEX-ADRIDMED (Mallet et al., 2015) and CHARMEX-SafMed, a large
86 coordinated effort of the French community has been recently conducted to better characterize the physico-
87 chemical properties of the Mediterranean atmosphere. Measurements were conducted at ground-stations on
88 Mediterranean islands, such as Crete (Finokalia) and Corsica (Ersa) for an extended period of the years 2013-
89 2014 and Mallorca (Cap Es Pinar) for several weeks during 2013. Forty airborne research flights were also
90 performed during the summers 2013 and 2014. This vast dataset gave us a unique opportunity to characterize the
91 spatial extent of the NPF process in the Mediterranean basin. In this paper, we first report long term analysis of
92 NPF event characteristics measured at Ersa (from May 2012 to August 2013) and Finokalia (from January to
93 December 2013) using size distribution measurements, in order to assess the large scale space and time
94 variability of NPF. We then focus our study on the Special Operation Period (SOP) that took place during
95 summer 2013. During this SOP additional measurements took place in Mallorca (from July 3rd to August 12th
96 2013) and aerosol particle size distributions and concentrations were measured onboard the ATR-42, which
97 allowed for a deeper analysis of the horizontal and vertical development of the NPF process at the daily scale.

98

99 **2 Experimental platforms, material and methods**

100 **2.1 Ground-based measurements**

101 Ground-based aerosol measurements reported in this work were performed at the Finokalia station (Crete) from
102 January to December 2013, at the Ersa station (Corsica) from May 2012 to August 2013, and at the Cap Es Pinar
103 station (Mallorca,) from July 3rd to August 12th 2013 (Figure 1). Within these measurements periods, some gaps
104 occurred in the Finokalia data set (from September 5th to October 15th 2013, 2013), due to participation of the
105 instrument in the ACTRIS (Aerosol Clouds and Trace gases Research Infrastructure) network mobility particle
106 size spectrometer workshop, and in the Ersa data set from September 1st to October 31th 2012), due to
107 instrumental failures.

108 The Finokalia station (35.24° N, 25.60° E) is located on the northern coast of Crete, Greece, at the top of a hill
109 (230 m a.s.l) facing the sea. There is no significant human activity within an area of approximately 15 km around
110 the station, mainly characterized by a scarce vegetation (Mihalopoulos et al., 1997). The closest large urban area
111 is the city of Heraklion, with 150 000 inhabitants, located 50 km West from Finokalia. Aerosols at the site are
112 mainly transported from the Southern-Eastern Europe and Northern Africa, and to a lesser extent from Central
113 and Western Europe (Kouvarakis et al., 2000; Sciare et al., 2008; Pikridas et al., 2010, 2012). At Finokalia,



114 aerosol particle size distributions were measured in the size range 8.8–848.7 nm, with a time resolution of 300 s,
115 with a custom-made Mobility Particle Size Spectrometer type (SMPS) (Wiedensohler et al., 2012). As
116 previously described by Kalivitis et al., (2015), the system operates with a closed-loop sheath air flow, with a 5:1
117 ratio between the sheath and the aerosol flow. It comprises a Kr-85 aerosol neutralizer (TSI 3077), a Hauke
118 medium differential mobility analyzer (DMA) and a TSI-3772 condensation particle counter (CPC). The system
119 is operated following the recommendations of Wiedensohler et al., (2012), thus meeting the European
120 infrastructure ACTRIS project requirements for quality insurance.

121 The Ersa station is located on the northern tip of Corsica Island, on Cape Corsica (43.00° N, 9.30° E, 530 m
122 a.s.l.). On this part of the island the wind can be very strong with frequent windstorms (78 days in 2007 with a
123 wind speed stronger than 28 m s⁻¹). Climate in Corsica is characterized by moist winters and dry summers, with
124 less than 100 rainy days per year (Lambert et al., 2009). Aerosols reaching the site are of variable types,
125 including mineral dust particles from North Africa, anthropogenic and biomass burning aerosols mainly
126 originating from densely populated coastal areas located in Eastern Spain, France and Italy, and marine aerosols,
127 both from the Mediterranean Sea itself but also from the Atlantic Ocean (Mallet et al., 2016; Nabat et al., 2013).
128 The Cape Corsica peninsula is a remote site, excluding important local anthropogenic sources that could affect
129 the in-situ measurements, and surrounded by a scarce Mediterranean vegetation (Mallet et al., 2016). At Ersa,
130 aerosol size distributions were measured with a scanning mobility particle sizer (SMPS TSI 3080, associated to a
131 CPC TSI 3010) in the size range 10.9–495.8 nm with a time resolution of 300 s.

132 The Cap Es Pinar station is located on the Northeastern side of the Mallorca Island (39.88° N, 3.19° E, 20 m
133 a.s.l.), on a peninsula between the Alcudia and Pollença bays. The station was placed in one of the buildings
134 belonging to the Spanish Ministry of Defense in his Cap Es Pinar facilities. The area is densely forested by
135 Mediterranean shrublands and pine trees and the access to the facilities is restricted. Urban centers, the Alcudia
136 and Pollença harbors and main roads are located at least 10 Km from the site. Particle size distributions were
137 measured in the size range 15–600 nm with a time resolution of 300 s using a TSI SMPS, with a 3081 long DMA
138 and a 3776 CPC.

139 2.2 Airborne measurements

140 Airborne measurements were carried out on board of the ATR-42, French research aircraft operated by SAFIRE
141 (Service des Avions Français Instrumentés pour la Recherche en Environnement). Figure 1 shows also the
142 aircraft trajectory during the flights performed on July 30th and August 1st which are investigated in the next
143 sections of the present work. The aerosol size distribution in the 20–485 nm diameter range was measured with a
144 time resolution of 130 s using the SMPS system previously described in (Crumeyrolle et al., 2010) which
145 includes a CPC (TSI, 3010), a differential mobility analyser (DMA) and a krypton aerosol neutralizer. The total
146 concentrations of aerosols larger than 10 nm (N₁₀) and larger than 3 nm (N₃) were measured using a custom-
147 made CPC dedicated to aircraft measurements (Weigel et al., 2009) and a CPC TSI 3025 type, respectively. The
148 concentration of particles in the size range 3 - 10nm (N₃₋₁₀) was calculated as the difference between N₃ and N₁₀.
149 After analysis of the variability of N₃₋₁₀ apart from nucleation periods, we found that N₃₋₁₀ concentrations are
150 above the variability of the two CPC concentration difference, corresponding to a threshold of 395 cm⁻³. For
151 more details on the airborne instrumentation and data analysis procedure, the reader is referred to Rose et al.,
152 (2015).



153

154 **3 Data analysis**

155 **3.1 NPF events classification**

156 From ground-based observations, NPF were classified according to Dal Maso et al (2005) into four categories:
157 events days, including classes I and II, undefined and non-events days. Class I events are characterized by a
158 strong increase of sub-25nm particles concentrations, their persistence over a period of more than an hour and a
159 clear growth of the nucleation mode particles towards larger sizes during the following hours. Class II events
160 have the same characteristics as Class I events, except that they may be less intense or show a discontinuity in
161 the growth of the clusters. Days are considered undefined when the newly observed particles are detected only
162 from the Aitken size and/or when they do not grow during the course of the day.

163 **3.2 Particle formation and growth rates calculations**

164 Particle formation and growth rates are key entities to assess the strength of events belonging to Class I and II.
165 Growth rates (GR) were calculated from the SMPS nucleation mode concentrations (16.3-20.2 nm) using the
166 “maxima” method from Hirsikko et al.(2005). The time corresponding to the maximum concentration was first
167 determined for each of the SMPS size channels in the range 16.3 – 20.2 nm by fitting a normal distribution to the
168 concentrations. The growth rate was then derived from a linear least square fit through these time values.

169 From this growth rate, we derived the total particle formation rate at 16 nm (J_{16}), similarly as in Dal Maso et
170 al. (2005) using the following equation (Eq.1) :

171

$$172 \quad J_{16} = \frac{dN_{16}}{dt} + CoagS_{16} * N_{16} + \frac{GR_{16.3-20.2}}{(20.2 - 16.3)nm} * N_{16} \quad (1)$$

173 $CoagS_{16}$ is the coagulation sink of 16 nm particles on larger particles, N_{16} is the total concentration of 16.3-20.2
174 nm particles and $GR_{16.3-20.2}$ is the growth rate corresponding to the same diameter range.

175

176 **4 Results and discussion**

177 **4.1 Yearly statistical analysis of NPF events characteristics at two ground-based stations**

178 The goal of this first section is to provide an overview of the seasonal variability of NPF in the Mediterranean
179 area, and some insights into the spatial homogeneity of the NPF occurrence over the basin.

180 **4.1.1 NPF Events frequency and types**

181

182 The yearly average NPF frequencies, calculated as the number of event days over the total number of
183 measurement days, are very similar at the two stations, being 36% and 35% at Finokalia and Ersu, respectively.
184 A comparable value is reported by Pikridas et al. (2012) at Finokalia, with a yearly average frequency around



185 33% calculated over a year from April 2008 to April 2009. At both stations, the NPF frequency shows a clear
186 annual cycle with the highest frequencies observed during spring (52% in May for Finokalia and 56% in April
187 for Ersa), and the lowest in autumn (Fig. 2). A similar seasonal variation was already reported for the Finokalia
188 station, with a slight time offset of the NPF frequency peak, which was found in February-March (Pikridas et al.,
189 2012). Higher NPF frequencies are frequently observed during spring (April-May-June) compared to the rest of
190 the year at European stations. They are mainly explained by the onset of biogenic emissions and increased solar
191 radiation (Manninen et al., 2010). The classification of the measurement days into the different categories (Fig.
192 3) shows that the occurrence of type I events in Finokalia follows the same seasonal variation as the total NPF
193 frequency, being maximum during the spring season (up to 26% of all days). This indicates that the spring
194 season is favorable to both formation of new particles and their growth to larger sizes. Type II events are
195 globally the most frequent, representing between 13% and 31% of all measurement days with no clear seasonal
196 variation. In contrast, undefined days are not frequently observed in Finokalia, around 9% on average. Very
197 similar features are observed in Ersa: type I events show the highest frequency of occurrence during spring and
198 summer (up to 32% of all days in August), while they represent less than 10% of the measurement days during
199 winter. The frequency of occurrence of type II events is on average 19%, with no clear seasonal variation.

200 4.1.2 Growth rates and particle formation rates

201 Particle formation and growth rates were calculated for type I events in order to characterize the strength of
202 the events observed at the different stations. The yearly median particle growth rates in the range 16 – 20 nm
203 (GR_{16-20}) are 7.10 and 16.7 nm h⁻¹ at Ersa and Finokalia, respectively (Table 1). The values obtained at Finokalia
204 are on average slightly higher compared to those reported by Manninen et al. (2010) in the range 7 – 20 nm (1.8
205 – 20 nm h⁻¹, mean value 4.4 nm h⁻¹). More generally, the values calculated in this work are on average slightly
206 higher compared to those obtained at other European coastal sites such as Cabauw (2.1 - 19 nm h⁻¹, mean value
207 6.7 nm h⁻¹) and Mace Head (2.7 – 10 nm h⁻¹, mean year value 5.4 nm h⁻¹) (Manninen et al., 2010). Figure 4
208 displays the annual variation of the particle growth rates (GR) at Ersa and Finokalia. At Ersa, the GR have the
209 same seasonal variation as the NPF frequency, with higher values in spring compared to the rest of the year. At
210 Finokalia, the GR seasonality is not as clear as in Ersa. However the seasonality in Finokalia is rather biased
211 because there are only few class I events during summer.

212 The yearly median particle formation rates are 0.16 cm⁻³s⁻¹ in Ersa and 0.26 cm⁻³s⁻¹ in Finokalia (Table 1). These
213 values are slightly lower than the J_{10} values reported by Kulmala et al. (2004) from several coastal sites and ship
214 campaigns conducted in the Baltic, Atlantic and Pacific areas (0.4 – 1.5 cm⁻³s⁻¹). The values calculated in this
215 work are, to our knowledge, the first reported for the formation of nucleation mode particles (10 – 20 nm) in the
216 Mediterranean basin. As reported on Fig. 5, the median J_{16} particle formation rates also follows a seasonal
217 variation similar to the NPF frequency at both stations, with higher values in spring (March with 0.56 cm⁻³s⁻¹ for
218 Finokalia, and April with 0.66 cm⁻³s⁻¹ for Ersa). In contrast, lower J_{16} are observed in early winter and mid-
219 summer at both stations. Available precursors for initiating nucleation in spring, presumably due to the onset of
220 biogenic emissions and increased solar radiation, are likely of the same origin than thus necessary for growing
221 clusters up to 16 nm.

222 It is worth noticing that in Ersa, even though NPF frequencies are weaker in autumn compared to spring,
223 particle formation rates are comparable. This last observation suggests that, despite being less frequent, favorable



224 conditions for NPF can be found during autumn and lead to events with the same intensity as in spring, when
225 radiation and biogenic emissions are on average higher compared to the rest of the year (Manninen et al., 2010).
226 Factors explaining the seasonal variation of nucleation frequency, nucleation rates and growth rates can be the
227 availability of condensable gases. The amount of such precursors results from a balance between a combination
228 of emissions and radiation that favor their production, and their loss onto preexisting particles. In order to assess
229 the influence of the preexisting aerosol population on NPF, we calculated the condensational sink (Cs) according
230 to Pirjola et al. (1999). The Cs was first derived from SMPS measurements for the whole measurement period at
231 both stations and was finally averaged over the two-hour period prior to the onset of NPF events. On non-event
232 days, the Cs was averaged over the two-hours time period prior to the mean time at which the NPF is triggered
233 on event days, i.e. around 11:00 (UTC) in Finokalia and 12:00 (UTC) in Ersa. The annual variation of the
234 median Cs derived from these averaged values is reported for event and non-event days on Fig. 6.

235 The Cs has a strong seasonal cycle with a clear maximum during summer at both stations. This observation may
236 explain the lower NPF frequencies, formation rates and growth rates that are on average observed during this
237 season, that otherwise shows high radiation and high biogenic emissions. In addition, at both stations, the Cs is
238 on average higher during non-event days. This confirms that the Cs is likely a limiting factor for the occurrence
239 of a NPF event at these stations. This was already pointed out by Hamed et al. (2010), Kulmala et al. (2005) and
240 Manninen et al. (2010) for the European atmosphere covering both the industrialized areas and boreal forest
241 environment respectively. The Cs is on average higher in Finokalia, especially during spring and summer with
242 monthly Cs twice as high compared to Ersa. It is worth noticing that large particles up to 848 nm are accounted
243 for in the Cs calculation in Finokalia, while the upper size limit is 495 nm in Ersa. However, particles above 500
244 nm only have a weak impact on the Cs values due to their low concentration, and thus do not explain the
245 differences which are seen between the sites. At Finokalia, N/NE winds dominate during summer, bringing high
246 concentrations of anthropogenic aerosol that have aged when passing over the sea before reaching the station,
247 thus leading to high Cs values. The fact that NPF frequencies, nucleation rates and growth rates are comparable
248 at the two stations indicates that the sources of condensable gases are likely to be significantly higher in
249 Finokalia compared to Ersa in order to compensate for the large condensational sink measured at the Crete
250 station.

251 Globally, Finokalia and Ersa show similar seasonality in the average nucleation frequency, growth rates and
252 nucleation rates although the two stations are more than 1000 km away from each other. It is worth mentioning
253 that during the period of interest, 104 event days were observed at Finokalia and 96 at Ersa, among which 31
254 (with 8 events of class I) occurred at both stations at the same time. These results could indicate that the spatial
255 extent of NPF events over the Mediterranean basin are of the order of magnitude of the distance between the two
256 stations. However, we will downscale the comparison of occurrence and characteristics of events at the daily
257 resolution (rather than monthly), in order to further investigate this hypothesis.

258 4.2 Intensive campaign during summer 2013

259 4.2.1 Ground-based measurements - overview



260 In this section, we focus on the Special Observation Period (SOP) that took place from June 3rd to August 12th in
261 the frame of the CHARMEX project. During this period, number size distribution measurements were
262 additionally conducted at the Mallorca station (Cap Es Pinar).

263 Figure 7 shows the SMPS particle size distributions recorded at the three ground-based stations during the SOP.
264 We clearly observe similar trends in the evolution of the particle size distributions in Ersa and Cap Es Pinar, with
265 three distinct NPF periods during which NPF events occurred daily over several days (First period from July 4th
266 to July 9th, second period from July 28th to August 3rd and third period from August 9th to August 12th) (see Table
267 S1). This observation would confirm the spatial extent of NPF events at a large scale. However, these periods of
268 intense NPF activity are not observed in Finokalia, where both the occurrence and strength of NPF events seem
269 to be more homogeneous over the SOP. These contrasting observations might be explained by an environmental
270 contrast between the eastern and western part of the Mediterranean basin.

271 In order to further investigate the link that might exist between the events observed at the three stations, we first
272 chose to focus our analysis on three specific days that belong to the three different NPF periods identified: July
273 5th, July 29th and August 9th are presented as case studies.

274 4.2.2 Ground-based measurements: Case studies

275 We calculated the total formation rate of 20 nm particles (J_{20}) using particle growth rates GR_{15-25} (Tab. 2) for the
276 three cases: July 5th, July 29th and August 9th. We first shortly describe the NPF events observed on the 5th and
277 29th of July (fully described in the supplementary) and then illustrate in more details the events observed on the
278 9th of August that have the most similarities between sites.

279 On July 5th, although NPF occurred both at Ersa and Cap Es Pinar, the time evolution of particle concentrations
280 are very different from one site to the other. Particles of the smallest size range are detected in the morning at
281 Ersa, but only later in the afternoon at Cap es Pinar, and at larger sizes and lower concentrations (Fig S1). The
282 24-hour air mass back trajectory analysis shows that air masses arriving at both stations are of northerly origin
283 (Fig S2). Hence it is unlikely that particles formed during the NPF event detected at Ersa in the morning have
284 been transported west and detected later in the afternoon at Cap Es Pinar. The calculation of the nucleation area
285 based on the NPF duration, growth rate and wind speed (see suppl. material), leads to a relatively small area of 9
286 km (Ersa) to 40 km (Cap Es Pinar), that does not allow further conclusions on the simultaneity of a large NPF
287 covering the spatial area of both stations. The event of July 29th was detected from the lowest sizes of the SMPS
288 at both stations with the same intensity (similar N_{15-20} and J_{20}), and show similar features (Fig. S3), but was
289 detected one hour earlier at Cap Es Pinar than at Ersa. Air masses were from the northern sector at Cap Es Pinar,
290 and then turned west towards Ersa (Fig. S5).

291 In Finokalia, both for July 5th and July 29th, significant N_{15-20} concentration are also detected during the
292 nucleation hours, but in the form of a succession of peaks that do not show the usual feature of a clear NPF event
293 (with a continuous growth).

294 On August 9th, newly formed particles are detected in air masses originating from the near Southern area in Ersa
295 and from Northwestern sector in Cap Es Pinar (Fig.9). The concentration of particles measured in the first SMPS
296 size channels in Ersa (11-15 nm) does not present very marked variations, while N_{15-20} displays more significant



297 changes in the course of the day. These observations might suggest that unlike previous events, NPF may not be
298 initiated at the station itself, but rather in a neighbouring area (Fig. 8). Similar features are observed at Cap Es
299 Pinar, with significant variations of the particle concentration in the size range 15-20 nm, as on July 29th. The
300 temporal evolutions of N_{15-20} and N_{20-25} have similar structures at both stations between 10:00 and 16:00 UTC,
301 suggesting that NPF could occur simultaneously at both sites. Additional peaks of N_{15-20} and N_{20-25} are detected
302 earlier in the morning at Cap Es Pinar (7:20 and 9:00 UTC), while they are not detected in Ersa. Beside the
303 simultaneity of the process, NPF events detected at the two sites also display very similar characteristics, both
304 regarding particle growth (4.3 and 3.8 nm h⁻¹, for Ersa and Cap Es Pinar, respectively) and formation rates (4.83
305 and 4.17 cm⁻³ s⁻¹, for Ersa and Cap Es Pinar, respectively). Instrumental failure did not allow similar analysis at
306 Finokalia. Figure 9 shows the estimate of the nucleation areas for the two stations. Concerning Cap Es Pinar, the
307 place where nucleation initially occurred is at least 49 km upstream the station.

308 Since all air mass back trajectories computed during the time period of interest are very local (at least during the
309 24 hours before their arrival at the site), we may hypothesise that NPF is occurring over the whole area close to
310 Mallorca where air mass backtrajectories overlap. Concerning Ersa, the nucleation of 20 nm particles latter
311 observed at the site is at least initiated 45 km upstream the station. The three case studies showed that NPF
312 events could be detected, with some time offset, on two remote stations separated by several hundred kilometers
313 in the Mediterranean area. In particular for the case of August 9th, the fact that these events can be detected in air
314 masses from different origins suggest that the NPF is, for both sites, initiated above the sea, either in the marine
315 boundary layer or higher in the free troposphere. In any case, the NPF process is likely not subject to the
316 availability of precursors that would be specific to the air mass type reaching the sites. It could rather depend on
317 synoptic meteorological conditions at the European scale, including low condensational sinks following
318 precipitations periods. Indeed, the analysis of the meteorological conditions along backtrajectories shows that
319 precipitation did occur prior to their arrival at both stations on July 29th (during the passage of low pressure
320 systems), but not on the two other case studies. The minimum areas that we determined for nucleation onset at
321 both sites do not overlap. However, the estimates we obtained are some lower limits of the actual values, and
322 there are no elements which could justify that the NPF is interrupted between both sites. Airborne measurements
323 will be used in the next section to further investigate this aspect. In addition, these flights will allow an analysis
324 regarding the origin of the clusters and their precursors, from the marine boundary layer or from the upper levels
325 of the atmosphere, as previously shown by Rose et al. (2015a).

326 4.2.3 Airborne measurements

327 Among the 11 flights performed during the period, particles in the lowest size range (N_{3-10}) were not observed
328 during 7 of the flights, in agreement with no NPF events detected at the Ersa and Cap Es Pinar stations. Two
329 flights detected elevated concentrations of N_{3-10} and N_{10-20} in agreement with NPF events at Ersa.

330 The first event to be investigated was observed on July 30th. Regarding aircraft measurements, the analysis was
331 focused on the flight legs performed at constant altitude and during which N_{3-10} concentrations were above the
332 threshold value (Fig 10a). The first part of the flight was performed at low altitude (~ 215 m a.s.l.) from the
333 french coast towards the Ersa station and at higher altitudes (~ 3400 m a.s.l.) during the second part of the flight
334 from the Ersa station towards the coast. Based on Fig. 10, small particles (N_{3-10}) were detected at both altitudes
335 and over a large area included in a 219 × 131 km rectangle. On the low altitude flight section, N_{3-10} are



336 decreasing from the Northeastern part of the flight track to the Southwestern one. This would indicate a source of
337 nanoparticles originating from the continent and progressively diluted in the marine boundary layer. However,
338 despite a high variability, N_{3-10} were on average higher at high altitude, with average concentrations of
339 $3805 \pm 1555 \text{ cm}^{-3}$ compared to $2040 \pm 2174 \text{ cm}^{-3}$ at lower altitude. This last observation supports the results of
340 Rose et al. (2015a) who reported that nucleation could be enhanced at high altitude above the Mediterranean Sea
341 and connected to different sources at low altitude.

342 In order to explore the link that may exist between the events detected simultaneously from the aircraft and from
343 the ground, we first investigated the origin of the air masses. Figure 10b shows the 72 hour back trajectories of
344 the air masses sampled by the ATR-42 every 10 min along the flight path as well as the 72 hour back trajectories
345 of the air masses that reached Ersá in the meanwhile at 13:00, 14:00 and 15:00 UTC. During the first part of the
346 flight performed at low altitudes, the aircraft flew in Southern air masses which all passed over the continent
347 before sampling and became more local as the aircraft approached Ersá. In contrast, the air masses sampled at
348 high altitude are from Western origin, so that they also passed over the continent, but did not display any local
349 features.

350 In addition, Fig. 11 shows the evolution of the particle size distributions measured onboard the ATR-42 and at
351 Ersá. The spectra are color coded according to the position of the aircraft indicated in the insert included in the
352 middle panel of Fig. 11. At Ersá, the shape of the particle size distribution remains similar during the whole
353 measurement period, with a nucleation mode around 20 – 25 nm, an Aitken mode around 50 – 60 nm which
354 clearly dominates the spectra and two accumulation modes, respectively around 110 and 220 nm. These modes
355 were identified when fitting the SMPS size distributions with four Gaussian modes using the methodology
356 described in Rose et al. (2015a). In contrast, the size distributions provided by the SMPS onboard the ATR-42
357 show significant variations. Lower concentrations are on average observed at higher altitude for the whole
358 diameter range but with more significant changes of the nucleation and Aitken modes. The shape of the size
359 distribution is also impacted by the location of the plane, especially at low altitude. In fact, the total particle
360 concentration decreases as the aircraft moves further off the southern coast of France, with, again, a more visible
361 impact on nucleation and Aitken modes.

362 These last observations, together with the air mass back trajectory analysis shown on Fig. 10.b, suggest that for
363 this first event, new particles were initially formed at low altitude over the continent and further transported
364 above the sea to be finally detected over a large area, and more especially in Ersá. Decreasing particle
365 concentrations observed while moving further off the continent make less probable the hypothesis of new small
366 particles formation from an additional marine source, but rather depict the effect of dispersion process that may
367 have taken place during particle transport.

368 The second event included in this analysis was observed on August 1st. Compared to the previous study case, the
369 flight was performed over a larger area ($172 \times 247 \text{ km}$ rectangle) located further away west from Ersá and at a
370 relatively low constant altitude ($\sim 500 \text{ m a.s.l.}$). N_{3-10} concentrations above the threshold value were detected
371 along the flight path (Fig. 12) and compared well, on average, with the concentrations obtained at low altitude
372 during the flight performed on July 30th ($2483 \pm 2767 \text{ cm}^{-3}$). However, N_{3-10} concentrations occurred as bursts,
373 with no clear spatial gradient as previously reported for flight performed on July 30th. The analysis of air mass
374 back trajectories is shown on Fig 12.b. North-Eastern air masses were sampled at the beginning and at the end of



375 the flight, with northern air masses in between. Air masses from the North were also detected at Ersa and it is
376 worth noticing that, at least during the first part of the flight, the air masses that reached the aircraft had all
377 passed over Ersa region.

378 The evolution of the particle size distributions together with the location of the aircraft is shown in Fig. 13.
379 Unlike during the flight performed on July 30th, the shape of the distributions measured onboard the ATR-42
380 remains similar during the whole measurement period despite the changing origin of air masses. In contrast, the
381 shape of the particle size distributions measured at Ersa shows a significant variability. Especially, the nucleation
382 mode displays increasing diameters from 20 to 30 nm and highly variable concentrations. Also, total
383 concentrations from Ersa are significantly higher compared to those measured onboard the ATR-42.

384 In order to further investigate the origin of the nucleation mode particles and the connection that may exist
385 between ground based and airborne measurements, we compared the diameters of the corresponding nucleation
386 modes. For that purpose, Fig. 14 shows the ratio of the nucleation mode diameter obtained onboard the ATR-42
387 over that from Ersa as a function of the distance between the aircraft and the station. This ratio is in the range 0.6
388 – 1.2, with on average decreasing values while increasing the distance between the two measurement points.
389 Nucleation mode diameter getting smaller along the air mass back trajectory above the sea could be the result of
390 intense inputs of nucleated particles initially below the SMPS size detection limit and feeding the nucleation
391 mode as they grow, as confirmed by the occurrence of N₃₋₁₀ nm particles detected in the ATR-42. In this
392 particular case, particles detected in the nucleation mode observed onboard the ATR-42 would be the result of an
393 event occurring above the sea from marine precursors, which superimposes with a preexisting particle mode.

394

395 **5 Conclusion**

396 We investigated the occurrence of NPF in the Mediterranean area using particle size distributions measured at
397 three ground-based stations (Ersa, Cap Es Pinar and Finokalia) as well as airborne measurements performed in
398 2012 – 2013 in the frame of the CHARMEX-ADRMED and CHARMEX-SafMed projects.

399 The analysis of long-term datasets from Ersa and Finokalia first revealed similar features, although the two
400 stations are more than 1000 km away from each other. Especially, almost equal annual NPF frequencies were
401 reported (36% and 35%, for Finokalia and Ersa, respectively) and similar seasonal variations of both the NPF
402 frequency and characteristics, i.e. particle formation and growth rates, were observed. The NPF process was on
403 average favored during spring, both in terms of occurrence and intensity, most probably because of increased
404 amounts of precursors from biogenic origin and higher solar radiation, thus allowing for more efficient
405 photochemistry processes.

406 This investigation, initially performed at a monthly resolution was downscaled in a second step at the daily
407 resolution over a two months period, in order to further better assess the simultaneity of NPF over a large part of
408 the Mediterranean basin. Three nucleation periods of several days appeared to clearly occur simultaneously at
409 Ersa and Cap Es Pinar, and less clearly at Finokalia. Three case study events were selected within these three
410 distinct NPF periods for a more detailed analysis. These three case studies showed that NPF events could be
411 detected, with some time offset, on two remote stations separated by several hundred kilometers in the



412 Mediterranean basin, without the stations being directly linked to each other within a single air mass trajectory.
413 While featuring local characteristics, the occurrence of NPF events was not likely dependant on the
414 availability of precursors that would be specific to the air mass type reaching the sites, but rather on synoptic
415 meteorological conditions at the European scale.

416 Airborne measurements were finally used to further investigate the horizontal and vertical extent of NPF, and to
417 determine the origin of the clusters and their precursors. Two case studies were again selected within the NPF
418 periods identified previously from ground-based observations, during which newly formed clusters were
419 observed onboard the ATR-42 and from Ersa on the same day. The selected events depicted contrasting
420 situations where particles were initially probably formed above the continent for one of them, both in the
421 boundary layer and in the free troposphere, and probably formed above the sea for the other. In each case,
422 clusters were detected over large areas confirming that NPF may be dependent on large scale processes.

423 This work, together with the previous study by Rose et al. 2015, demonstrates the occurrence of NPF in the
424 Mediterranean basin, thus highlighting the possibility for the process to be triggered above open seas. Those
425 results are of great interest to improve the parameterizations of nucleation in models, which actually only
426 consider a limited number of precursors, commonly including sulfuric acid and ammonia but excluding those
427 more specifically emitted in the marine atmosphere. Model predictions would also benefit from the analysis of
428 the vertical extent of the NPF process provided in these studies. Besides the identification of preferential
429 altitudes for the occurrence of the process, these results aid understanding the transport of the newly formed
430 clusters and their precursors between the boundary layer and the free troposphere. Future studies should focus on
431 understanding the chemical precursors that contribute to these new particle formation processes.

432 Acknowledgements

433 This study was performed with the financial support of the French National Research Agency (ANR) project
434 ADRIMED (contract ANR-11-BS56-0006) the ANR project SAF-Med "" (Grant Number: SIMI-5-6 022 04) and
435 is part of the ChArMEX project supported by ADEME, CEA, CNRS-INSU and Météo-France through the
436 multidisciplinary programme MISTRALS (Mediterranean Integrated Studies at Regional And Local
437 Scales). The Financial support for the ACTRIS Research Infrastructure Project by the European Union's Horizon
438 2020 research and innovation program under grant agreement no. 654169 and previously Under grant agreement
439 no. 262254 in the 7th Framework Programme (FP7/2007–2013) is gratefully acknowledged.

440

441 References

442 Birmili, W., Berresheim, H., Plass-Dülmer, C., Elste, T., Gilge, S., Wiedensohler, A. and Uhrner, U.: The
443 Hohenpeissenberg aerosol formation experiment (HAFEX): a long-term study including size-resolved aerosol, H
444 2 SO 4, OH, and monoterpenes measurements, *Atmospheric Chem. Phys.*, 3(2), 361–376, 2003.

445 Crippa, P. and Pryor, S. C.: Spatial and temporal scales of new particle formation events in eastern North
446 America, *Atmos. Environ.*, 75, 257–264, doi:10.1016/j.atmosenv.2013.04.051, 2013.

447 Crumeyrolle, S., Manninen, H. E., Sellegri, K., Roberts, G., Gomes, L., Kulmala, M., Weigel, R., Laj, P. and
448 Schwarzenboeck, A.: New particle formation events measured on board the ATR-42 aircraft during the
449 EUCAARI campaign, *Atmospheric Chem. Phys.*, 10(14), 6721–6735, doi:10.5194/acp-10-6721-2010, 2010.

450 Cusack, M., Pérez, N., Pey, J., Alastuey, A. and Querol, X.: Source apportionment of fine PM and sub-micron
451 particle number concentrations at a regional background site in the western Mediterranean: a 2.5 year study,
452 *Atmospheric Chem. Phys.*, 13(10), 5173–5187, doi:10.5194/acp-13-5173-2013, 2013.



- 453 Dal Maso, M., Kulmala, M., Riipinen, I., Wagner, R., Hussein, T., Aalto, P. P. and Lehtinen, K. E. J.: Formation
454 and growth of fresh atmospheric aerosols : eight years of aerosol size distribution data from SMEAR II,
455 Hyytiälä, Finland, *Boreal Environ. Res.*, 10(5), 323–336, 2005.
- 456 Dall’Osto, M., Querol, X., Alastuey, A., O’Dowd, C., Harrison, R. M., Wenger, J. and Gómez-Moreno, F. J.: On
457 the spatial distribution and evolution of ultrafine particles in Barcelona, *Atmospheric Chem. Phys.*, 13(2), 741–
458 759, doi:10.5194/acp-13-741-2013, 2013.
- 459 Hamed, A., Birmili, W., Joutsensaari, J., Mikkonen, S., Asmi, A., Wehner, B., Spindler, G., Jaatinen, A.,
460 Wiedensohler, A., Korhonen, H. and others: Changes in the production rate of secondary aerosol particles in
461 Central Europe in view of decreasing SO₂ emissions between 1996 and 2006, *Atmospheric Chem. Phys.*, 10(3),
462 1071–1091, 2010.
- 463 Hirsikko, A., Laakso, L., Hörrak, U., Aalto, P. P., Kerminen, V.-M. and Kulmala, M.: Annual and size
464 dependent variation of growth rates and ion concentrations in boreal forest, *Boreal Environ. Res.*, 10(5), 357–
465 369, 2005.
- 466 Hirsikko, A., Bergman, T., Laakso, L., Maso, M. D., Riipinen, I., Horrak, U. and Kulmala, M.: Identification and
467 classification of the formation of intermediate ions measured in boreal forest, *Atmospheric Chem. Phys.*, 7(1),
468 201–210, 2007.
- 469 Hussein, T., Junninen, H., Tunved, P., Kristensson, A., Dal Maso, M., Riipinen, I., Aalto, P. P., Hansson, H.-C.,
470 Swietlicki, E. and Kulmala, M.: Time span and spatial scale of regional new particle formation events over
471 Finland and Southern Sweden, *Atmos Chem Phys*, 9(14), 4699–4716, 2009.
- 472 Jeong, C.-H., Hopke, P. K., Chalupa, D. and Utell, M.: Characteristics of Nucleation and Growth Events of
473 Ultrafine Particles Measured in Rochester, NY, *Environ. Sci. Technol.*, 38(7), 1933–1940,
474 doi:10.1021/es034811p, 2004.
- 475 Kalivitis, N., Birmili, W., Stock, M., Wehner, B., Massling, A., Wiedensohler, A., Gerasopoulos, E. and
476 Mihalopoulos, N.: Particle size distributions in the Eastern Mediterranean troposphere, *Atmospheric Chem.*
477 *Phys.*, 8(22), 6729–6738, 2008.
- 478 Kalivitis, N., Stavroulas, I., Bougiatioti, A., Kouvarakis, G., Gagné, S., Manninen, H. E., Kulmala, M. and
479 Mihalopoulos, N.: Night-time enhanced atmospheric ion concentrations in the marine boundary layer,
480 *Atmospheric Chem. Phys.*, 12(8), 3627–3638, doi:10.5194/acp-12-3627-2012, 2012.
- 481 Kalivitis, N., Kerminen, V.-M., Kouvarakis, G., Stavroulas, I., Bougiatioti, A., Nenes, A., Manninen, H. E.,
482 Petäjä, T., Kulmala, M. and Mihalopoulos, N.: Atmospheric new particle formation as a source of CCN in the
483 eastern Mediterranean marine boundary layer, *Atmos Chem Phys*, 15(16), 9203–9215, doi:10.5194/acp-15-9203-
484 2015, 2015.
- 485 Koren, I., Dagan, G., Altartaz, O. and others: From aerosol-limited to invigoration of warm convective clouds,
486 *Science*, 344(6188), 1143–1146, 2014.
- 487 Kouvarakis, G., Tsigaridis, K., Kanakidou, M. and Mihalopoulos, N.: Temporal variations of surface regional
488 background ozone over Crete Island in the southeast Mediterranean, *J. Geophys. Res. Atmospheres* 1984–2012,
489 105(D4), 4399–4407, 2000.
- 490 Kristensson, A., Johansson, M., Swietlicki, E., Kivekäs, N., Hussein, T., Nieminen, T., Kulmala, M. and Dal
491 Maso, M.: NanoMap: Geographical mapping of atmospheric new particle formation through analysis of 1
492 particle number size distribution data 2 3 Short version of title: “NanoMap: Mapping of new particle formation
493 events” 4 5, [online] Available from: <http://www.cast.lu.se/Kristensson%20-%20NanoMap%20paper%20v4.pdf>
494 (Accessed 14 March 2016), 2014.
- 495 Kulmala, M., Vehkamäki, H., Petäjä, T., Dal Maso, M., Lauri, A., Kerminen, V.-M., Birmili, W. and McMurry,
496 P. H.: Formation and growth rates of ultrafine atmospheric particles: a review of observations, *J. Aerosol Sci.*,
497 35(2), 143–176, 2004.



- 498 Kulmala, M., Petäjä, T., Mönkkönen, P., Koponen, I. K., Dal Maso, M., Aalto, P. P., Lehtinen, K. E. J. and
 499 Kerminen, V.-M.: On the growth of nucleation mode particles: source rates of condensable vapor in polluted and
 500 clean environments, *Atmos Chem Phys*, 5, 409–416, 2005.
- 501 Makkonen, R., Asmi, A., Kerminen, V.-M., Boy, M., Arneth, A., Hari, P. and Kulmala, M.: Air pollution control
 502 and decreasing new particle formation lead to strong climate warming, *Atmospheric Chem. Phys.*, 12(3), 1515–
 503 1524, doi:10.5194/acp-12-1515-2012, 2012.
- 504 Mallet, M., Dulac, F., Formenti, P., Nabat, P., Sciare, J., Roberts, G., Pelon, J., Ancellet, G., Tanré, D., Parol, F.,
 505 Denjean, C., Brogniez, G., di Sarra, A., Alados-Arboledas, L., Arndt, J., Auriol, F., Blarel, L., Bourrienne, T.,
 506 Chazette, P., Chevaillier, S., Claeys, M., D'Anna, B., Derimian, Y., Desboeufs, K., Di Iorio, T., Doussin,
 507 J.-F., Durand, P., Féron, A., Freney, E., Gaimoz, C., Goloub, P., Gómez-Amo, J. L., Granados-Muñoz, M. J.,
 508 Grand, N., Hamonou, E., Jankowiak, I., Jeannot, M., Léon, J.-F., Maillé, M., Mailler, S., Meloni, D., Menut, L.,
 509 Momboisse, G., Nicolas, J., Podvin, T., Pont, V., Rea, G., Renard, J.-B., Roblou, L., Schepanski, K.,
 510 Schwarzenboeck, A., Sellegri, K., Sicard, M., Solmon, F., Somot, S., Torres, B., Totems, J., Triquet, S., Verdier,
 511 N., Verwaerde, C., Waquet, F., Wenger, J. and Zapf, P.: Overview of the Chemistry-Aerosol Mediterranean
 512 Experiment/Aerosol Direct Radiative Forcing on the Mediterranean Climate (ChArMEx/ADRIMED) summer
 513 2013 campaign, *Atmospheric Chem. Phys.*, 16(2), 455–504, doi:10.5194/acp-16-455-2016, 2016.
- 514 Manninen, H. E., Nieminen, T., Asmi, E., Gagné, S., Häkkinen, S., Lehtipalo, K., Aalto, P., Vana, M., Mirme,
 515 A., Mirme, S., Hörrak, U., Plass-Dülmer, C., Stange, G., Kiss, G., Hoffer, A., Törö, N., Moerman, M., Henzing,
 516 B., de Leeuw, G., Brinkenberg, M., Kouvarakis, G. N., Bougiatioti, A., Mihalopoulos, N., O'Dowd, C.,
 517 Ceburnis, D., Arneth, A., Svenningsson, B., Swietlicki, E., Tarozzi, L., Decesari, S., Facchini, M. C., Birmili,
 518 W., Sonntag, A., Wiedensohler, A., Boulon, J., Sellegri, K., Laj, P., Gysel, M., Bukowiecki, N., Weingartner, E.,
 519 Wehrle, G., Laaksonen, A., Hamed, A., Joutsensaari, J., Petäjä, T., Kerminen, V.-M. and Kulmala, M.:
 520 EUCAARI ion spectrometer measurements at 12 European sites – analysis of new particle formation events,
 521 *Atmos Chem Phys*, 10(16), 7907–7927, doi:10.5194/acp-10-7907-2010, 2010.
- 522 Merikanto, J., Spracklen, D. V., Mann, G. W., Pickering, S. J. and Carslaw, K. S.: Impact of nucleation on global
 523 CCN, *Atmospheric Chem. Phys.*, 9(21), 8601–8616, 2009.
- 524 Mihalopoulos, N., Stephanou, E., Kanakidou, M., Pilitsidis, S. and Bousquet, P.: Tropospheric aerosol ionic
 525 composition in the Eastern Mediterranean region, *Tellus*, 49B, 314–326, 1997.
- 526 Nabat, P., Somot, S., Mallet, M., Chiapello, I., Morcrette, J. J., Solmon, F., Szopa, S., Dulac, F., Collins, W.,
 527 Ghan, S., Horowitz, L. W., Lamarque, J. F., Lee, Y. H., Naik, V., Nagashima, T., Shindell, D. and Skeie, R.: A
 528 4-D climatology (1979–2009) of the monthly tropospheric aerosol optical depth distribution over the
 529 Mediterranean region from a comparative evaluation and blending of remote sensing and model products,
 530 *Atmospheric Meas. Tech.*, 6(5), 1287–1314, doi:10.5194/amt-6-1287-2013, 2013.
- 531 Pey, J., Rodríguez, S., Querol, X., Alastuey, A., Moreno, T., Putaud, J. P. and Van Dingenen, R.: Variations of
 532 urban aerosols in the western Mediterranean, *Atmos. Environ.*, 42(40), 9052–9062,
 533 doi:10.1016/j.atmosenv.2008.09.049, 2008.
- 534 Pikridas, M., Bougiatioti, A., Hildebrandt, L., Engelhart, G. J., Kostenidou, E., Mohr, C., Prévôt, A. S. H.,
 535 Kouvarakis, G., Zarrmpas, P., Burkhart, J. F., Lee, B.-H., Psychoudaki, M., Mihalopoulos, N., Pilinis, C., Stohl,
 536 A., Baltensperger, U., Kulmala, M. and Pandis, S. N.: The Finokalia Aerosol Measurement Experiment – 2008
 537 (FAME-08): an overview, *Atmospheric Chem. Phys.*, 10(14), 6793–6806, doi:10.5194/acp-10-6793-2010, 2010.
- 538 Pikridas, M., Riipinen, I., Hildebrandt, L., Kostenidou, E., Manninen, H., Mihalopoulos, N., Kalivitis, N.,
 539 Burkhart, J. F., Stohl, A., Kulmala, M. and Pandis, S. N.: New particle formation at a remote site in the eastern
 540 Mediterranean, *J. Geophys. Res. Atmospheres*, 117(D12), D12205, doi:10.1029/2012JD017570, 2012.
- 541 Pirjola, L., Kulmala, M., Wilck, M., Bischoff, A., Stratmann, F. and Otto, E.: FORMATION OF SULPHURIC
 542 ACID AEROSOLS AND CLOUD CONDENSATION NUCLEI: AN EXPRESSION FOR SIGNIFICANT
 543 NUCLEATION AND MODEL COMPARISON, *J. Aerosol Sci.*, 30(8), 1079–1094, doi:10.1016/S0021-
 544 8502(98)00776-9, 1999.
- 545 Rose, C., Sellegri, K., Freney, E., Dupuy, R., Colomb, A., Pichon, J.-M., Ribeiro, M., Bourrienne, T., Burnet, F.
 546 and Schwarzenboeck, A.: Airborne measurements of new particle formation in the free troposphere above the



- 547 Mediterranean Sea during the HYMEX campaign, *Atmospheric Chem. Phys.*, 15(17), 10203–10218,
548 doi:10.5194/acp-15-10203-2015, 2015.
- 549 Rosenfeld, D., Sherwood, S., Wood, R. and Donner, L.: Climate Effects of Aerosol-Cloud Interactions, *Science*,
550 343(6169), 379–380, doi:10.1126/science.1247490, 2014.
- 551 Sihto, S.-L., Kulmala, M., Kerminen, V.-M., Maso, M. D., Petäjä, T., Riipinen, I., Korhonen, H., Arnold, F.,
552 Janson, R., Boy, M. and others: Atmospheric sulphuric acid and aerosol formation: implications from
553 atmospheric measurements for nucleation and early growth mechanisms, *Atmospheric Chem. Phys.*, 6(12),
554 4079–4091, 2006.
- 555 Sciare, J., K. Oikonomou, O. Favez, Z. Markaki, E. Liakakou, H. Cachier, and N. Mihalopoulos, Long-term
556 measurements of carbonaceous aerosols in the Eastern Mediterranean: Evidence of long-range transport of
557 biomass burning, *Atmos. Chem. Phys.*, 8, 5551–5563, 2008
- 558 Spracklen, D. V., Carslaw, K. S., Kulmala, M., Kerminen, V.-M., Sihto, S.-L., Riipinen, I., Merikanto, J., Mann,
559 G. W., Chipperfield, M. P., Wiedensohler, A., Birmili, W. and Lihavainen, H.: Contribution of particle formation
560 to global cloud condensation nuclei concentrations, *Geophys. Res. Lett.*, 35(6), doi:10.1029/2007GL033038,
561 2008.
- 562 Tao, W.-K., Chen, J.-P., Li, Z., Wang, C. and Zhang, C.: Impact of aerosols on convective clouds and
563 precipitation, *Rev. Geophys.*, 50(2), doi:10.1029/2011RG000369, 2012.
- 564 Weigel, R., Hermann, M., Curtius, J., Voigt, C., Walter, S., Böttger, T., Lepukhov, B., Belyaev, G. and
565 Borrmann, S.: Experimental characterization of the CCondensation PArticle counting System for high altitude
566 aircraft-borne application, *Atmospheric Meas. Tech.*, 2, 243–258, 2009.
- 567 Wiedensohler, A., Birmili, W., Nowak, A., Sonntag, A., Weinhold, K., Merkel, M., Wehner, B., Tuch, T.,
568 Pfeifer, S., Fiebig, M., Fjåraa, A. M., Asmi, E., Sellegri, K., Depuy, R., Venzac, H., Villani, P., Laj, P., Aalto, P.,
569 Ogren, J. A., Swietlicki, E., Williams, P., Roldin, P., Quincey, P., Hüglin, C., Fierz-Schmidhauser, R., Gysel, M.,
570 Weingartner, E., Riccobono, F., Santos, S., Gröning, C., Faloon, K., Beddows, D., Harrison, R., Monahan, C.,
571 Jennings, S. G., O'Dowd, C. D., Marinoni, A., Horn, H.-G., Keck, L., Jiang, J., Scheckman, J., McMurry, P. H.,
572 Deng, Z., Zhao, C. S., Moerman, M., Henzing, B., de Leeuw, G., Löschau, G. and Bastian, S.: Mobility particle
573 size spectrometers: harmonization of technical standards and data structure to facilitate high quality long-term
574 observations of atmospheric particle number size distributions, *Atmospheric Meas. Tech.*, 5(3), 657–685,
575 doi:10.5194/amt-5-657-2012, 2012.
- 576 Yli-Juuti, T., Riipinen, I., Aalto, P. P., Nieminen, T., Maenhaut, W., Janssens, I. A., Claeys, M., Salma, I.,
577 Ocskay, R. and Hoffer, A.: Characteristics of new particle formation events and cluster ions at K-pusztá,
578 Hungary, *Boreal Environ. Res.*, 14(4), 683–698, 2009.
- 579 Yli-Juuti, T., Nieminen, T., Hirsikko, A., Aalto, P. P., Asmi, E., Hörrak, U., Manninen, H. E., Patokoski, J., Dal
580 Maso, M., Petäjä, T., Rinne, J., Kulmala, M. and Riipinen, I.: Growth rates of nucleation mode particles in
581 Hyytiälä during 2003−2009: variation with particle size, season, data analysis method and ambient
582 conditions, *Atmospheric Chem. Phys.*, 11(24), 12865–12886, doi:10.5194/acp-11-12865-2011, 2011.
- 583 Young, L.-H., Benson, D. R., Montanaro, W. M., Lee, S.-H., Pan, L. L., Rogers, D. C., Jensen, J., Stith, J. L.,
584 Davis, C. A., Campos, T. L., Bowman, K. P., Cooper, W. A. and Lait, L. R.: Enhanced new particle formation
585 observed in the northern midlatitude tropopause region, *J. Geophys. Res.*, 112(D10),
586 doi:10.1029/2006JD008109, 2007.
- 587
- 588



588

589

590 **Tables**591 **Table.1 Annual median formation rate, annual growth rate and annual Cs, with percentiles in Ersa and Finokalia.**

	$J_{16} (\text{cm}^{-3} \text{s}^{-1})$			$GR_{16-20} (\text{nm.h}^{-1})$			$Cs (\text{s}^{-1})$		
	25 th perc.	med.	75 th perc.	25 th perc.	med.	75 th perc.	25 th perc.	med.	75 th perc.
Ersa	1.4×10^{-1}	1.6×10^{-1}	3.0×10^{-1}	6.6	7.1	12.2	3.3×10^{-3}	4.1×10^{-3}	4.6×10^{-3}
Finokalia	1.9×10^{-1}	2.6×10^{-1}	2.8×10^{-1}	10.4	16.7	25.6	3.4×10^{-3}	6.2×10^{-3}	9.3×10^{-3}

592

593 **Table 2: Average growth rates and formation rates computed for individual events at Ersa and Mallorca**

595

	Ersa		Mallorca	
	$GR_{16-20} \text{nm.h}^{-1}$	$J_{16} \text{cm}^{-3} \text{s}^{-1}$	$GR_{16-20} \text{nm.h}^{-1}$	$J_{16} \text{cm}^{-3} \text{s}^{-1}$
July 5 th	16.4	2.44×10^{-1}	7.8	0.41×10^{-1}
July 29 th	8.9	7.88×10^{-2}	4.8	7.75×10^{-2}
August 9 th	4.3	4.83×10^{-2}	3.8	4.17×10^{-2}



596

597

598 **Figures**

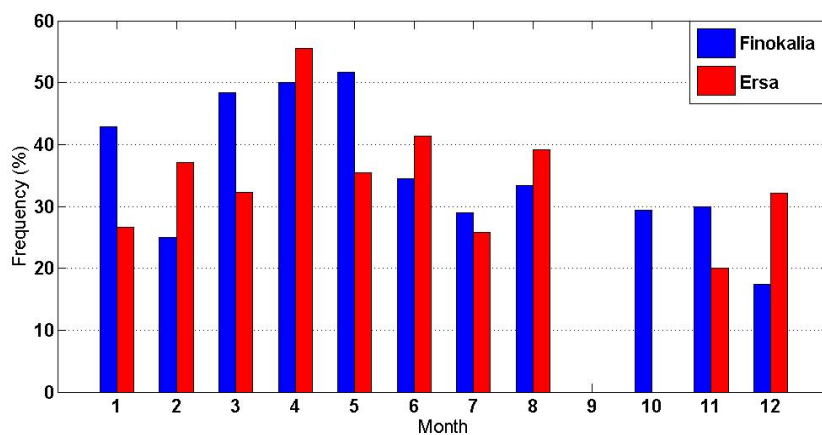
599



600

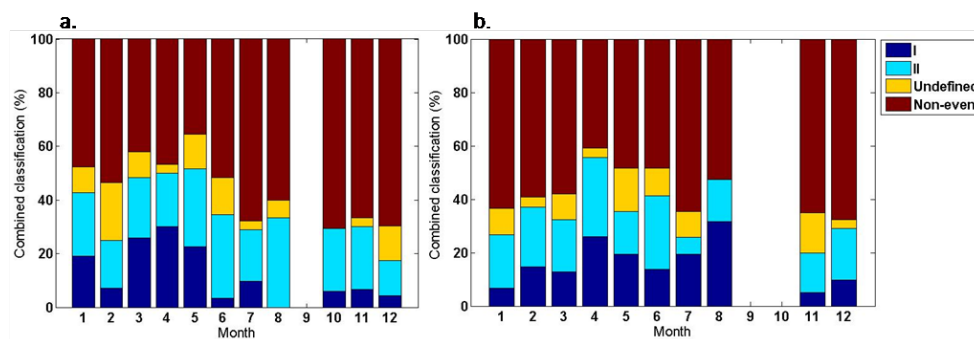
601 **Figure 1:** Localization of stations Ersá (Corsica), Finokalia (Crete) and Cap Es Pinar (Mallorca) and of the aircraft
602 flight paths on July 30th and August 1st.

603



604

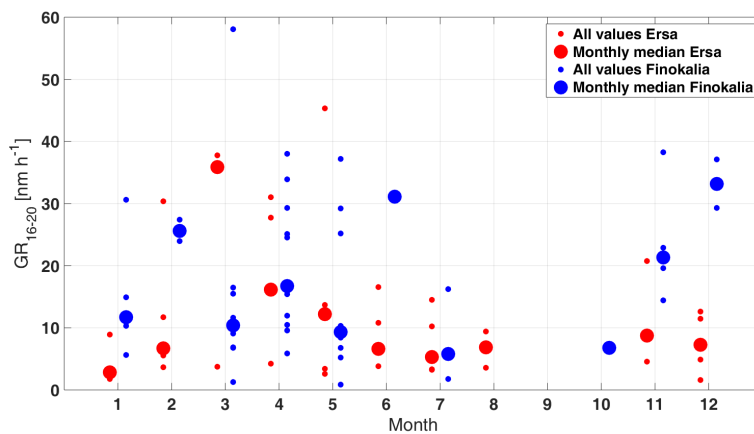
605 **Figure 2:** Monthly mean (January to December) NPF frequencies at Finokalia and Ersá.



606

607 **Figure 3: Monthly classification of the days into event (I and II), undefined and non-event categories in Finokalia (a)**
608 **and Ersä (b)**

609



610

611

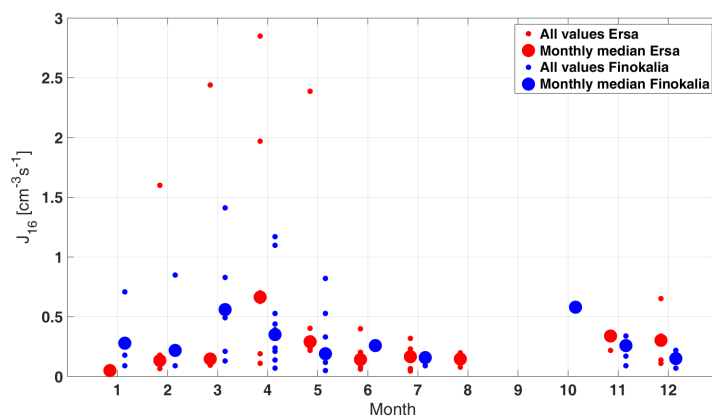
612 **Figure 4: Annual variation of particle growth rate calculated for the range 16 – 20 nm at Ersä (May 2012 – August**
613 **2013) and Finokalia (January – December 2013) for type I events. Small dots represent all values while large dots**
614 **stand for median values.**

615

616

617

618



619

620 **Figure 5:** Annual variation of the 16 nm particle formation rate calculated for the range 16 – 20 nm at Erska (May
 621 2012 – August 2013) and Finokalia (January – December 2013) for type I events. Small dots represent all values while
 622 large dots stand for median values.

623

624

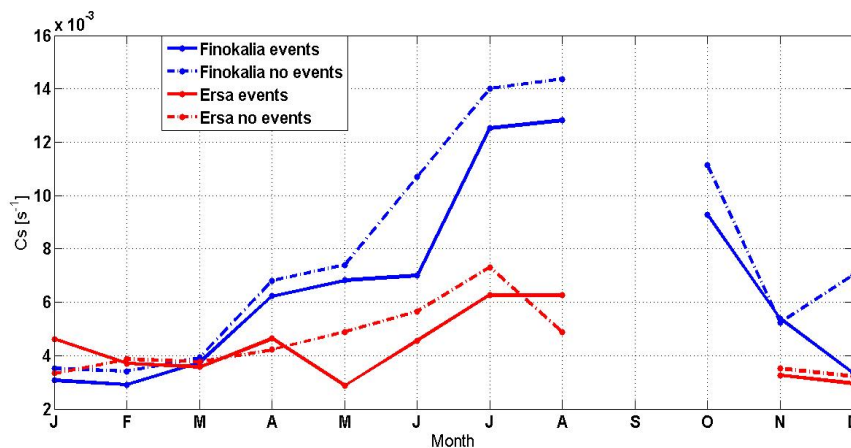
625

626

627

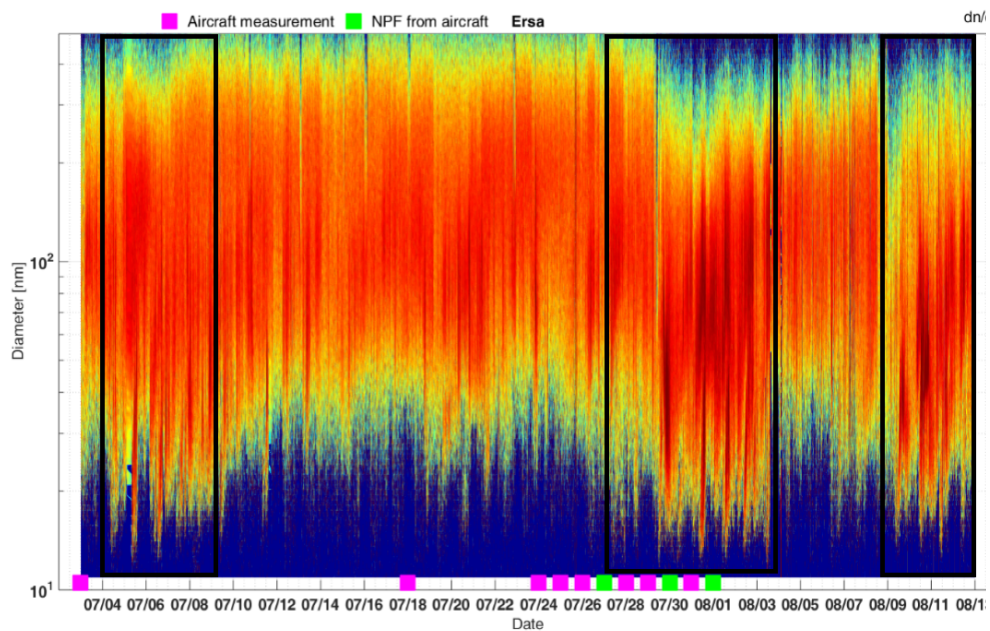
628

629

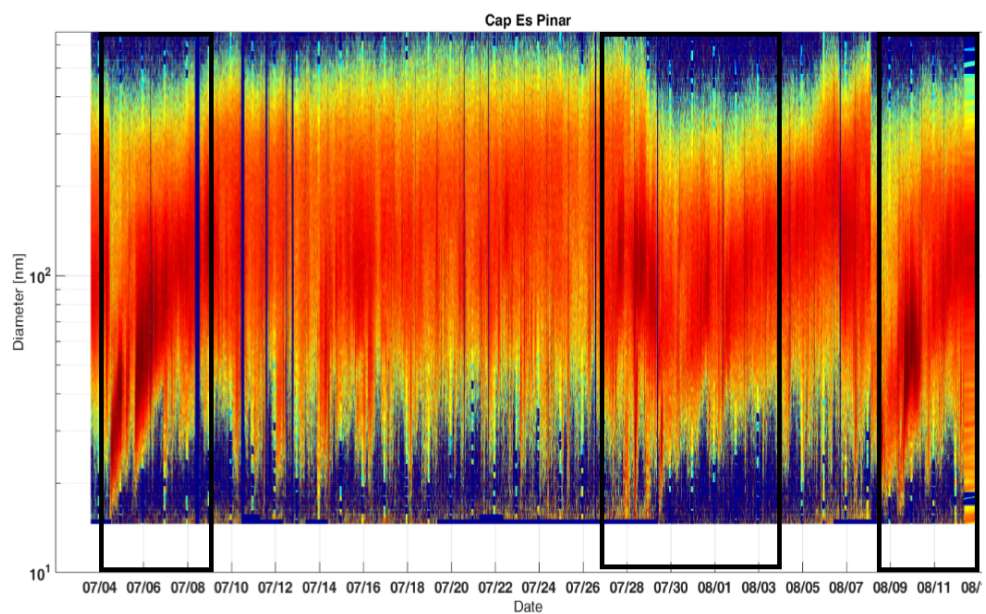


630

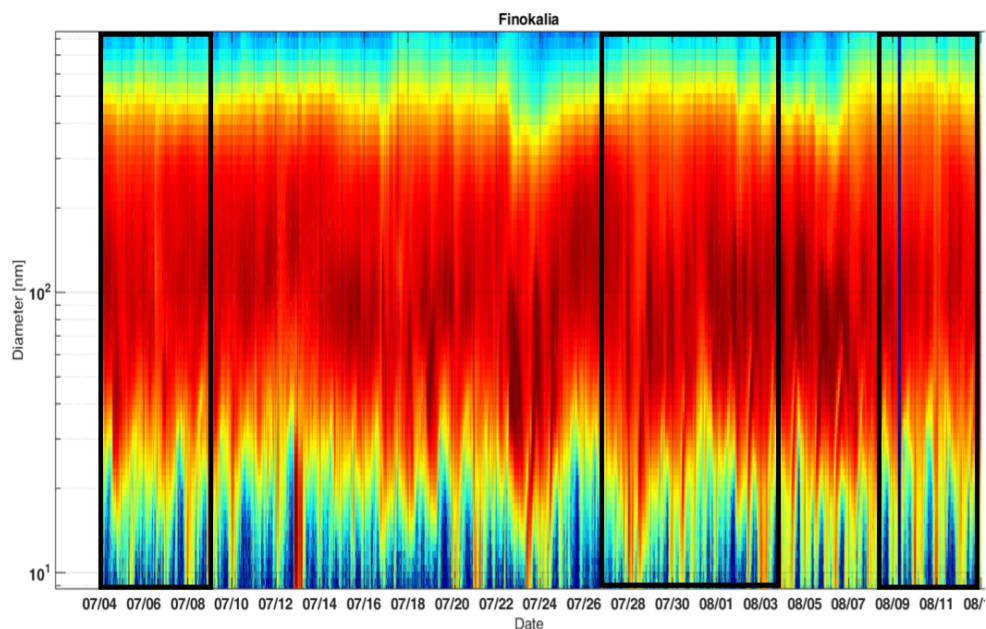
631 **Figure 6:** Median values of condensation sink (Cs) during event and non-event days in Finokalia and Erska.



632



633



634

635 **Figure 7:** SMPS particle number size distribution in Finokalia, Ersá and Cap Es Pinar (Mallorca) during the intensive
636 campaign. The three NPF episodes observed at large scale are marked on the spectra in the black boxes. The days of
637 occurrence of the ATR-42 flights are also shown, together with the detection of NPF from these airborne
638 measurements.

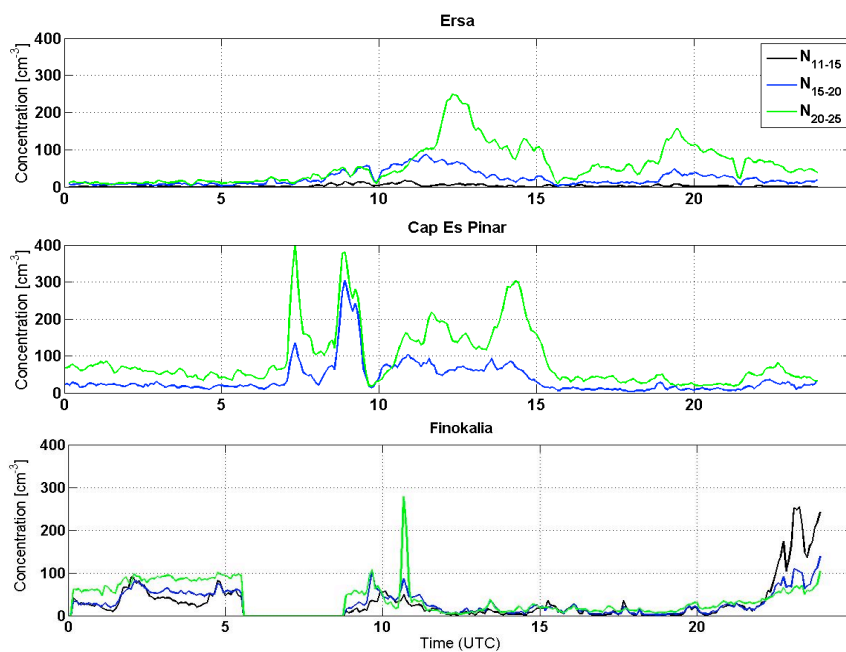


Figure 8: Temporal evolution of the particle concentrations in the size range 11-15 nm (black) (N_{11-15}), 15-20 nm (blue) (N_{15-20}) and 20-25 nm (green) (N_{20-25}) for August 9th event.



639

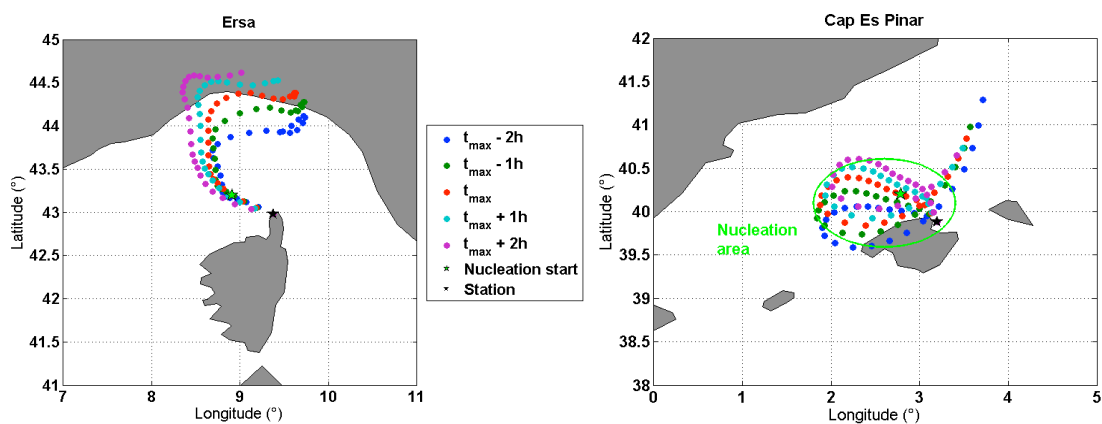
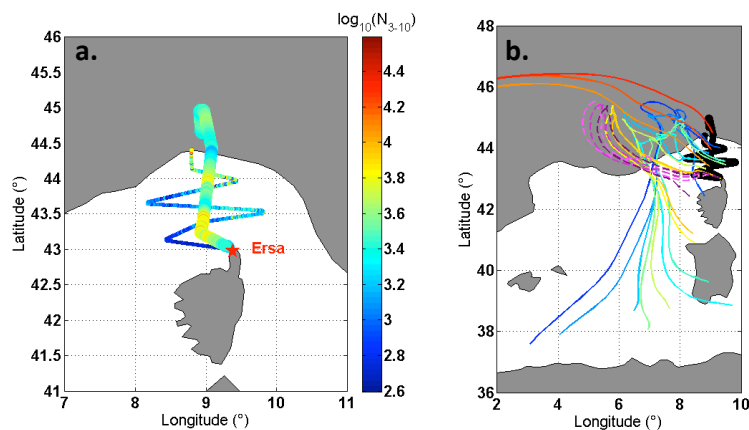


Figure 9: Backtrajectories of air masses sampled in Ersa and Cap Es Pinar on August 9th at t_{max} , when 20 nm particles concentration is maximum, and during the two hours that precede and follow this maximum. The location where nucleation initially occurs upstream the station is marked with a green star.

640

641

642



643

644 Figure 10: a. N_{3-10} above the threshold value along the flight path performed on July 30th. Large size dots stand for
 645 high altitude measurements (~ 3400 m a.s.l.) while small size dots stand for low altitude measurements (~ 215 m a.s.l.);
 646 b. Air mass back trajectories calculated along the flight path (black line) every ten minutes together with the back
 647 trajectories of air masses arriving in Ersa each hour during the same time period (dashed lines).

648

649

650

651



652

653

654

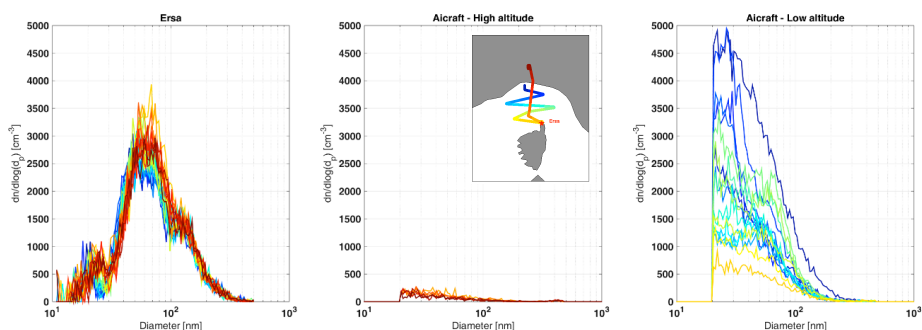
655

656

657

658

659

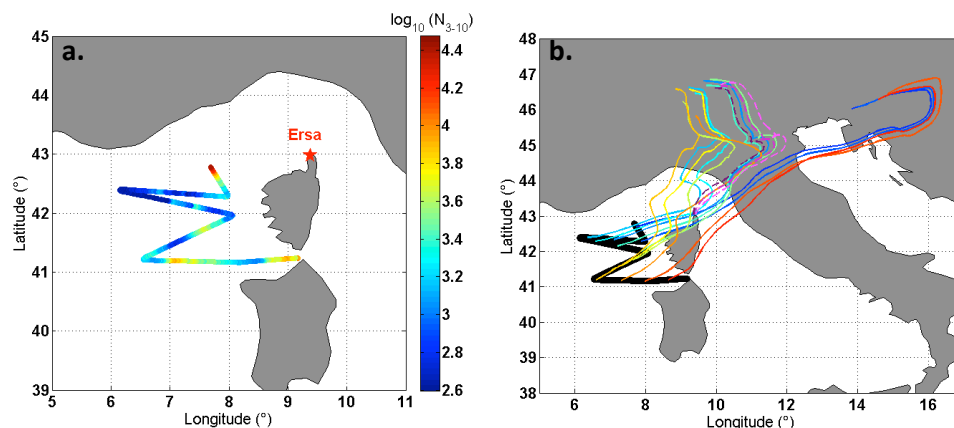


660 **Figure 11: SMPS size distributions measured at the Ersa station (left panel) and on board of the ATR-42 at high**
661 **altitudes (~ 3400 m a.s.l.) (middle panel) and low altitude (~ 215 m a.s.l.) (right panel) on July 30th.** The color coding
662 of the size distributions corresponds to the location of the aircraft, as shown on the insert of the middle panel.

663

664

665



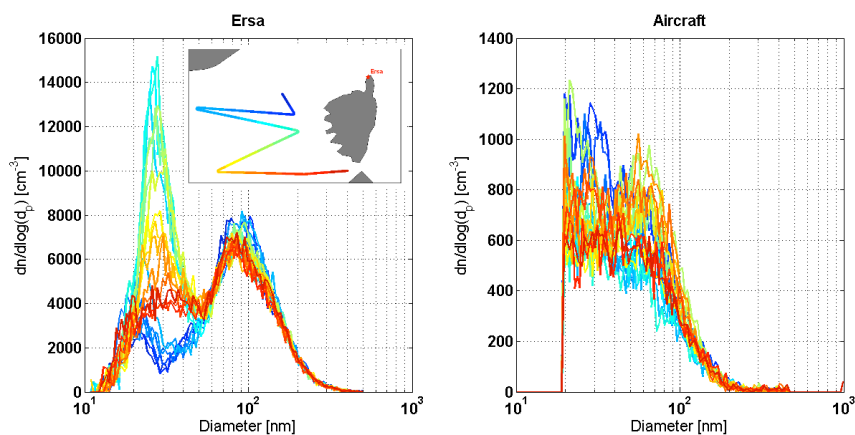
666

667 **Figure 12: a. N_{3-10} above the threshold value along the flight path; b. Air mass back trajectories (solid lines) calculated**
668 **along the flight path (black line) every ten minutes together with the back trajectories of air masses arriving in Ersa**
669 **each hour during the same time period (dashed lines) during the August 1st flight.**

670

671

672



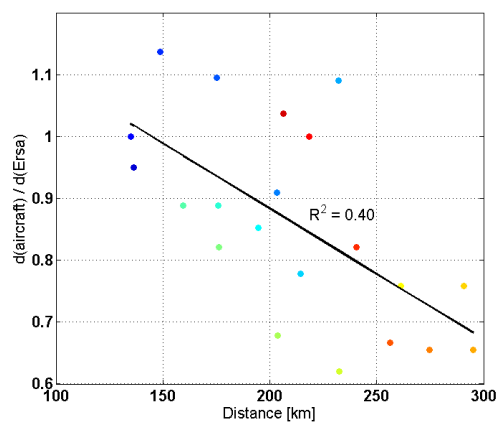
673

674 **Figure 13: Ground based (left panel) and airborne (right panel) SMPS size distributions measured on August 1st. The**
675 **color coding of the spectra corresponds to the location of the aircraft, as shown on the insert of the left panel.**

676

677

678



679

680 **Figure 14: Ratio of nucleation mode diameters measured onboard the ATR-42 over that calculated in Ersa as a**
681 **function of the distance between the aircraft and Ersa for August 1st. The color coding of this scatter plot matches**
682 **with the location of the aircraft showed on the insert of the left panel figure 13.**

683

684